Mesoporous and Mesostructured Materials for Optical Applications

Brian J. Scott,*,† Gernot Wirnsberger,‡ and Galen D. Stucky†

Department of Chemistry and Biochemistry, University of California, Santa Barbara, Santa Barbara, California 93106, and Department of Chemistry, Inorganic Chemistry, Karl-Franzens-University Graz, 8010 Graz, Austria

Mesostructured and mesoporous materials are emerging as a new class of optical materials. For mesostructured materials (inorganic/surfactant composites), prepared using a one-step synthesis procedure where the inorganic/surfactant/optically active species coassemble, the unique architecture provided by the surfactant−inorganic phase separation allows for higher concentrations compared to traditional sol−gel glasses and protective packaging of uniform three-dimensional arrays of optical species. The corresponding regularly arranged pores found in mesoporous materials (inorganic only) provide a high surface area to better disperse optically active components and allow for rapid diffusion for optical sensor applications. In this review, we discuss recent research results on the techniques used to produce optically functionalized mesostructured and mesoporous materials and the characterization of the final composites.

Introduction

In the early 1990s, the announcement by Kato and co-workers[1] and Mobil Research and Development Corporation[2] of a new class of materials called FSM and MCM led to a new synthesis strategy for preparing mesoporous materials. Previously, chemists and material scientists had used individual molecules to control the properties of porous materials, for example zeolites. Instead, Kato and the Mobil researchers used supramolecular templating and coassembly to produce ordered mesoporous silica with high surface area and pore sizes from 2 to 10 nm. Over the next few years, extensive research was carried out to make the materials more stable, expand the pore size, extend the framework composition, and examine new supramolecular templates. As a result of these efforts, it is currently possible to produce mesoporous materials with pore sizes from 2 to 50 nm[3,4] and to synthesize mesoporous transition metal oxides,[5–9] metal sulfides,[10–15] and hybrid silica/organic frameworks.[16–19] Further, to control processing conditions to make films,[20–25] fibers,[26] monoliths,[27–29] and other interesting shapes (e.g., gyroids),[30,31] optically defined structures using photoacids,[32] and by combining with soft lithography and polymer spheres to make hierarchically patterned materials.[33,34]

The large pore size, high surface area, and thermal stability of the FSM and MCM family instantly created interest in using these materials as catalysts and supports. More recently, mesoporous and mesostructured materials have attracted interest for electronic and optical applications. It has been recognized that mesoporous systems are promising candidates for the next-generation low-*k* dielectric materials for integrated

circuits.[19,35] In the field of optical materials, mesostructured materials fall in the range between nanoporous host such as zeolites that can align small molecules[48] and patterned micron-scale photonic band gap materials. However, the mesopore size range does have several possible advantages for optical applications. The high surface area creates the potential to dope materials at higher concentrations without interactions. The meso size range, 2−50 nm, is attractive for producing size-confined structures such as quantum dots[36–41] or nanowires.[42–44] Further, the highly uniform porosity of the mesoporous materials allows for facile diffusion, thereby making them excellent hosts for sensing molecules/ions.

The as-synthesized mesostructured materials, i.e., materials in which the organic templates are not removed, have recently been examined for the low-temperature synthesis of optical materials by using dye doping. For sol−gel glasses, low-temperature dye doping was reported nearly two decades ago, and subsequent research has led to the introduction of optically active sol−gel glasses into the market.[45] However, all the advantages of sol−gel glasses (high dye dispersion, mechanical robustness, transparency of the matrix in the visible to UV range, high processability, etc.) are also present in mesostructured materials. Moreover, as we will outline below, simultaneous silica/block copolymer/dye coassembly can lead to improved optical characteristics. The key point is the nanoscopic structure built up by the organic/inorganic phase separation. For example, in the silica poly(ethylene oxide)−poly(propylene oxide)−poly(ethylene oxide) (PEO−PPO−PEO) triblock copolymers, coassembly leads to ordered inorganic/organic arrays on the nanometer length scale with uniform inorganic wall thickness. These nanostructures, of which a schematic example is depicted in Figure 1, provide different environments to the dyes incorporated

---

† University of California, Santa Barbara.
‡ Karl-Franzens-University Graz.
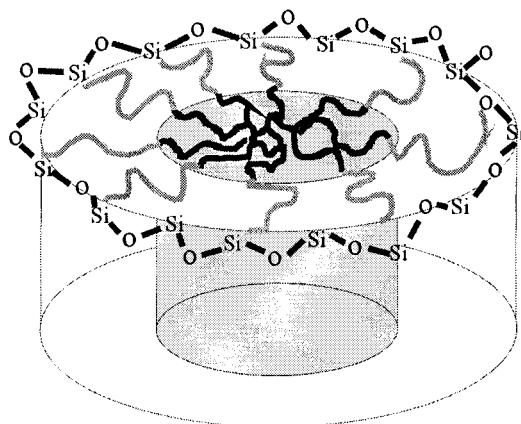* To whom correspondence should be addressed. E-mail: scott@chem.ucsb.edu.

Figure 1. Schematic illustration of a hexagonal silica/block copolymer mesostructure showing the polypropylene oxide/ poly(ethylene oxide)/silica nanophase separation.

during synthesis. From that viewpoint, a block copolymer/ silica mesostructure can be regarded as a system containing three chemical "subphases"—the hydrophobic PPO block, the hydrophilic PEO block, and the silica wall—whereby the PEO block also extends into the silica wall.[27] Of course, the occlusion of a dye into preferentially one or maybe more subphases will be determined by chemical interactions like electrostatic forces, hydrogen bonding, and dispersion forces.

This short review attempts to cover the optical properties of doped mesoporous and hybrid mesostructured material. The review is organized to take the reader from early results emphasizing the possible ways and different materials used for doping mesoporous materials to results on research directly aimed at applications. We have tried to make this review as comprehensive as possible, and we apologize in the event we were not successful in this regard. This review does not cover synthesis[46] and catalytic applications[47] of mesoporous materials or optical properties of sol–gel[45] and molecular seize (zeotype) materials,[48] which are described elsewhere.

Early Work: Dye Inclusion

Early research in optical properties of mesostructured and mesoporous materials grew on the success of dye doping in polymers,[49] sol–gel inorganic matrices,[45,50–52] and molecular sieve materials.[48] Mesostructured materials offer the same rigidity and photostability while at the same time having a well-defined hydrophilic/ hydrophobic phase separation allowing for more sophisticated tuning of the dye microenvironment. One of the first reports of dye-doped mesostructured materials was by Zhou et al. This group utilized the surfactant's potential to solubilize organic molecules in hopes of producing periodic arrays of chlorophyll in MCM-41.[53] By adding small amounts into the synthesis, they made 2d hexagonally ordered materials with an absorption spectrum similar to the dye in solution. Simultaneously, they extended the synthesis of hexagonal MCM type silica by using a redox active surfactant, 11-ferrocenyl-trimethylundecylammonium (ferrocenyl TMA).[54] Ferrocenyl TMA was selected because it can solubilize organic molecules in its tail and has a similar headgroup

as the alkylamine previously used. In addition to the redox active surfactant, they codoped the system with copper phthalocyanine (CuPc). Adsorption spectra revealed that the surfactant exists in both the original reduced state and an oxidized state from reacting with air. Further, the hydrophobic portion of the surfactant allowed for incorporation of a higher concentration of CuPc with little aggregation as suggested by only slight broadening of the adsorption spectrum. They have since progressed to mesoporous transition metal oxides and found photocatalytic activity for Pc-doped WO_3.[55] Hoppe et al. investigated doping rhodamine-B into MCM-41 synthesis and reported spectroscopic properties of the dye/surfactant/silica composite and physical properties of the calcined silica powders.[56] Spectroscopic studies of rhodamine B doped composites revealed a high monomer concentration relative to dimer, confirming the power of the coassembly process and an increased pore size of the MCM-41 solid upon calcination.

Calcined mesoporous powders can make excellent hosts for dye adsorption. This was demonstrated by Yamashita et al., who incorporated doping rhodamine-B into mesoporous powders of MCM-41 and titanium-doped MCM-41 structures.[57] Lifetimes of the dyes doped onto the MCM structures were longer than those on silica gel or in the microporous host ZSM-5. Later, Gu et al. thermally doped MCM-41 with coumarin 540 and studied the photoluminescence spectral properties.[58] Under excitation at 483 nm, the emission from the coumarin 540 was red-shifted relative to the dye in ethanol. The red shift was attributed to an increase in the polarity of the dye's environment caused by the silanols on the surface of the mesopore. Further, the emission's lifetime was measured by a multifrequency phase fluorometer with excitation at 360 nm and was reduced from 5.2 ns in ethanol to 3.5 ns on the mesopore. They suggested the decreased lifetime resulted from interactions with the surface silanols instead of dynamic quenching, dye–dye interactions.

The first group to successfully form ordered mesoporous materials with the dye covalently attached to the inorganic wall was done by Mann and co-workers. By adding small amounts of 3-(2,4-dintirophenylamino)-propyl(triethoxy)silane into the synthesis followed by surfactant removal by ethanol extraction, they synthesized 2d hexagonally ordered porous powders.[59] Shifts in absorption properties of the attached dye lead them to conclude that the dye was located predominately in the pore. More importantly, the emission characteristics of the dye were maintained. Later, the same research group extended their synthesis from powders to thin films and monoliths.[60] This was a fundamental step for the production of chemical sensors, which will be discussed later.

Later, Ganschow et al. developed a technique for anchoring dye molecules onto powders using microwave-assisted hydrothermal co-condensation.[61] After first synthesizing dye functionalized silicon alkoxides [RSi-$(OC_2H_5)_2$ where R is an azo or rhodamine dye] and diluting with tetraethyl orthosilicate [TEOS], the silicate precursors were added to basic water template solutions and heated using microwaves. The rapid microwave heating allowed for significant reductions in

synthesis times, thereby preventing dye degradation. The final powders were 2d hexagonally ordered silicates belonging to the MCM-41 family. The template could then be extracted under acidic conditions while the dye remained covalently linked to the framework. They were able to successfully incorporate both azo and rhodamine dyes, and retain the dye's optical activity. For example, the rhodamine dye could be loaded at high concentrations without forming low quantum yield dimers. However, a decrease in fluorescence intensity was observed at high concentrations attributed to radiationless energy transfer, Förster quenching.

A final way to introduce dyes into mesoporous materials was developed by Shibata et al.[62] On the basis of smectite research,[63] they dopped calcium ions into mesoporous materials and used the ion−dye interactions to hold the dyes onto the solid. Photostability studies were conducted by painting the powders onto paper, exposing to sunlight, and then measuring the color change using a colorimeter. They found that direct synthesis of calcium-modified MCM materials provided better dye photostability compared to samples made by ion exchange.

Nanocrystals

Another mechanism for generating optical mesostructured materials is to utilize the organized pores as hosts for growing or depositing inorganic materials. Specifically, the idea is to use the mesopores, 4−50 nm, to generate ordered arrays of semiconductor nanocrystals, quantum dots. It is well-known that as semiconducting materials decrease in size, their optical properties drastically change as quantum confinement occurs.[64] The most notable feature is a blue shift in the emission spectrum of the nanocrystals that is tunable with size. In the hopes of utilizing ordered uniform nanometer size mesopores, several groups have developed techniques for depositing semiconductors in the mesoporous materials.

Some of the early examples involved metal−organic vapor deposition (MOCVD) to grow III−V quantum-confined structures. Srdanov et al.[37] and Agger et al.[41] simultaneously grew GaAs and InP nanocrystals, respectively. Both groups synthesized siliceous MCM-41 structures, which were then loaded into MOCVD reactors for growth. Optical investigations of GaAs nanocrystals showed a luminescence shift of 0.1 eV attributed to quantum confinement. However, the observation of a broad spectrum at low temperatures was suggestive of a large size distribution. The size distribution was explained by two possible phenomena. The first was that while the mesoporous host confines diameter growth no confinement in length exist. This allows for morphologies ranging from nearly spherical nanocrystals up to 2d quantum-confined rods to exist. Experimentally, this was suggested by the emission dependence of the excitation, since different size quantum dots adsorb and emit at different wavelengths. The second reason was that crystallites must also exist on the surface of the mesopore. For InP, NMR, X-ray diffraction, TEM, and optical measurements were used to show quantum confinement for a fraction of the particles. Extensive experiments revealed similar data to the GaAs case in that evidence existed for both size-confined nanostructures and bulk material deposited on the surface on the mesostructures.

In 1995, Leon et al. developed a slight modification of the MOCVD method to make germanium nanocrystals.[65] They used an elimination reaction of digermane (Ge_2H_6) with the hydroxyls of siliceous mesoporous materials to synthesize size confined germanium. The germanium location was conclusively determined by a detailed transmission electron microscopy (TEM) study and found that the germanium nanocrystals were inside the mesopores. Later, Ozin and co-workers improved upon this scheme to produce size-confined silicon clusters.[66] Instead of using the empty mesopores as a template, the reactivity of the inorganic walls of as-made mesostructured thin films were explored. They used the hydrophobicity of the organic surfactant to allow gas-phase precursors to diffuse into the dense as-made material. Once Si_2H_6 diffuses into the mesostructure, it reacts with the silanols on the surface of the inorganic silica phase, providing a nucleation site for the silicon clusters. The uniqueness of this technique is not only does it use the as-made film structures but also comparatively low temperatures (100−140 °C). The silica walls and the surfactant then limit the sizes of the silicon clusters. By carefully controlling the reaction conditions, quantum-confined silicon clusters (~1 nm) can be synthesized that exhibit a yellow-orange photoluminescence. The low-temperature synthesis conditions employed in combination with the easily processed films represent an important step toward low-temperature optical devices.

Zhang et al. used principles similar to those developed for germanium and silicon to produce ZnO clusters.[40] ZnO is a wide band-gap semiconductor and is of interest for short-wavelength electrooptic devices. After first synthesizing and calcining siliceous MCM-41 material, ethylenediamine groups were grafted onto the surface. The ethylenediamine groups were then used to coordinate zinc ions from solutions before converting to ZnO by heating to 600 °C. X-ray and TEM studies showed that the mesoporous structure was maintained after treatment. The presence of ZnO was confirmed by diffuse-reflectance spectra, changes in gas adsorption properties, and elemental analysis using EDS. Unlike previous studies, no large aggregates were found by TEM, suggesting only small nanoparticles were made. Analysis of diffuse-reflectance spectra suggested ZnO nanoparticles to be ~1.8 nm, well within the size range expected for the 2.62 nm pores. Luminescence spectra were blue-shifted due to quantum confinement and centered around 450 nm. The luminescent sites were attributed to oxygen vacancies. The authors attempted to generalize the technique for other metal oxides or noble metals, but with the exception of cobalt oxide, were unsuccessful at obtaining the isolation found in ZnO.

Winkler et al. used a slightly different approach to produce quantum-confined nanostructures.[38] Instead of reacting calcined powders with gas-phase molecules at high temperatures, they loaded the pores with an organometallic single molecular precursor that decomposes to produce semiconductor materials. Originally, they focused on synthesizing wide band-gap group III nitrides because of their technological importance in blue/violet light-emitting diodes (LEDs) and lasers. Boron-doped MCM-41 was dehydrated and then loaded with triazido(trimethylamine)gallium. The sample was

then heated to 500 °C under ammonia to decompose the complex and form GaN. By controlling loading concentrations and washing procedures, they were able to control the amount of GaN deposited on the surface relative to that in the mesopores. While all samples showed a blue-shifted excitation onset along with a bulk excitation, extensive washing reduced the signal of bulk GaN. Estimates of the band gap in reference to the 2.7 nm pore size gave good agreement with experimental evidence, suggesting that the final composites had GaN inside the pores. Later, the same research group used a more conventional method of wet impregnation and organometallic decomposition to grow CdSe quantum dots inside mesoporous silica.[36] This time, mesoporous silica was added to a synthesis used to make colloidal CdSe.[67] By including mesoporous silica along with the dimethylcadmium and selenium, they were able to control the delivery and nucleation of the nanocrystals to be predominately inside the pores.

A final way to incorporate semiconductor nanocrystals is to first synthesize the nanoparticles and then adsorb them inside the mesoporous host (MCM-41). This type of synthesis has been used for CdS. CdS nanocrystals were grown in inverse micelles and then mixed with thiol functionalized mesoporous silica with different pore sizes.[39] By comparing the absorption spectra of the supernatant before and after addition of mesoporous silica, size selective incorporation of quantum dots was observed. Pore confinement was then inferred by analysis of the diffuse-reflectance spectra of the CdS/mesoporous material. For the large and medium sized mesoporous samples, the nanocrystal size was less than the pore size. However, the small sized mesopore sample had nanocrystals adhere to either the exterior silica surface or inside macropores, which were found by gas adsorption. Photocatalytic studies of H_2 production by the CdS/mesoporous material showed that the largest pore sized material had the largest activity. Unfortunately, no emission spectra were reported.

Organometallic Complexes

Not only do the mesoporous materials offer unique possibilities for doping with nanocrystals, but also the opportunity exists to load them with luminescent organometallic complexes. This has been by reported by Ogwa et al., who loaded tris(2,2′-bipyridine)ruthenium-(II) ([Ru(bpy)$_3$]$^{2+}$) complexes into mesoporous silica to investigate its nature as an immobilizing agent.[68] Experiments found that as the mesoporous silica was dehydrated, the luminescence from the complex was reduced. Further, when rehydrated, the luminescence intensified. From these observations, it was suggested that the adsorbed [Ru(bpy)$_3$]$^{2+}$ aggregated in the mesopore upon dehydration, causing self-quenching. Upon subsequent adsorption of water, the [Ru(bpy)$_3$]$^{2+}$ was dispersed. These data suggest that the [Ru(bpy)$_3$]$^{2+}$ adsorbs to the mesopore framework only by very weak interactions.

Simultaneously, Xu et al. investigated rare earth complexes loaded into mesoporous materials.[69] Rare earth complexes are known to be very sensitive to their local environments and therefor offer the ability to probe their surrounding. By loading [Eu(TTA)$_4$]$^{3+}$ (where TTA is 1-(2-thenoyl)-3,3,3-trifluoracetate) into two different

mesoporous materials, differences in emission spectra were observed. One sample consisted of an unmodified MCM-41 mesoporous material. The emission peaks of the complex were found to be similar to the complex in solution. In the second sample, the walls of the mesopores were modified with ethylenediamine groups. The effect of this modification was to reduce luminescence quenching by the hydroxyls on the surface and to reduce pore size from 29.31 to 14.26 Å. Since the [Eu(TTA)$_4$]$^{3+}$ complex is ∼12 Å, the reduced pore size allows for more hydrogen bonding between the walls and the complex. This increase in bonding slightly decreases the symmetry of the europium and causes a large enhancement of the $^5D_0 \rightarrow {}^7F_2$ (612 nm) transition, thereby improving the color purity. This transition is well know to be a hypersensitive transition in europium complexes and therefore particularly responsive to local environment.[70,71] Further, they note that the photostability for the complex is enhanced in the modified mesoporous material compared to solution and that a longer lifetime is observed.

Polymer Inclusions

The first successful attempt at using the pore orientation to produce optical materials occurred by doping mesoporous materials with semiconducting polymers. Tolbert and co-workers synthesized ordered mesoporous silica with aligned pores using magnetic fields.[72] They then modified the surface with organic groups to reduce the pore opening and make the silica hydrophobic before infiltrating poly[2-methoxy-5(2′-ethoxyhexloxy)-1,4-phenylenevinylene] (MEH-PPV) into the pores by thermal cycling. The group carefully chose the polymer and mesopore size to ensure that only a single chain could fit within the pores. Polarization studies demonstrated MEH-PPV was orientated greater than 80% in the mesoporous host (Figure 2). Further, the encapsulated polymer was found to be more thermally stable than the polymer on the surface.[73]

Later, Tolbert and co-workers used their ability to isolate individual polymer chains between a thick dielectric to study the polymer's photophysics and energy transfer through the polymer.[74] By using femtosecond pump−probe spectroscopy, they demonstrated that the dynamics of the states reached by excited-state absorption of the polymer chains inside the pores follow that of highly excited isolated chains in solution, whereas the excited states of the polymer chains on the surface were similar to that of spun-coated thin films. Time-resolved luminescence studies showed controlled energy transfer by measuring the time-dependent luminescence anisotropy (the difference in intensity between light emitted parallel and perpendicular to the pores when excited with a constant polarized source). The anisotropy initially underwent an ultrafast decay attributed to interchain energy transfer from randomly orientated polymer outside the pores. Temporally, this is followed by a slow increase in anisotropy assigned to luminescence from polymer segments aligned inside the pores, strongly suggesting direct energy transfer from the randomly orientated exterior to the aligned polymer chains inside the mesopores. The rationale behind these observations is that conjugation length affects the rate of energy transfer within the polymer. The driving force
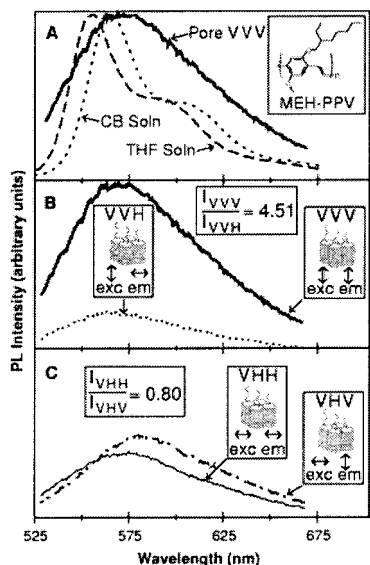
Figure 2. (A) Steady-state PL spectra of MEH-PPV in different environments: dashed curve is chlorobenzene (CB) solution, dotted curve is THF solution, mesoporous silica with exicitation and collection parallel to the pore diameter. (B) PL of MEH-PPV in nanostructured composite with excitation (exc) polarized along the pore direction. The heavy curve shows emission (em) collected with polarization along the pore direction. The dotted curve shows emission collected with polarization along the perpendicular to the pore direction. (C) PL of MEH-PPV in nanostructured composite with excitation (exc) polarized perpendicular to the pore direction. The dotted curve shows emission (em) collected with polarization along the pore direction. The thin curve shows emission collected with polarization along the perpendicular to the pore direction.

for this energy transfer arose from the changes in polymer conformation. The short conjugation length segments outside the mesoporous silica have higher energy than the long conjugation length segments inside the pores. The authors showed that intrachain energy transfer is a much slower process than interchain energy transfer. This is in contrast to carrier transport where intrachain mobility is several orders of magnitude larger than interchain. This study clearly demonstrated the utility of aligned mesopores by showing that energy transfer is conformation driven in MEH-PPV. More importantly, they produced a synthetic system where the flow of energy could be controlled and set the groundwork for investigating new nanoengineered mesopore polymer devices.

NLO and Laser Materials

Building on their success in zeotype materials,[75] Marlow and co-workers demonstrated the first potential application of doped mesoporous materials.[76] After first synthesizing siliceous MCM-41 and boron-doped MCM-41, the nonlinear optical (NLO) dye *p*-nitroaniline (pNA) was incorporated into the pores by vapor phase and alcoholic solutions. Orientation dependence of the X-ray diffraction peaks assigned to pNA suggested the dye molecules were arranged as a quasi-one-dimensional crystal with its long axis parallel to the long axis of the mesopore channel. In addition, other reflections were observed for pNA molecules stacked with different orientations. Second harmonic generation (SHG) measurements found that fresh samples displayed no SHG

activity. However, after aging for several weeks at ambient conditions, the vapor phase loaded samples showed an increased one-dimensional ordering by X-ray diffraction and SHG. The absolute value of nonlinear susceptibility was $X^2_{av} \sim 3$ pm/V and is comparable to KDP. Further experiments showed the aging process could be significantly reduced by exposure to high humidity. From these observations, it was proposed that in freshly prepared samples ordered was well as the disorder pNA in the pores average their dipoles locally and therefore are centrosymmetric and do not exhibit SHG. After aging, water coadsorption causes some of the disordered parts of pNA to rearrange. This results in the X-ray diffraction intensifying from more ordered pNA in the composite and SHG.

On the basis of the preliminary dye doping results, mesostructured materials are promising candidates for solid state dye lasers. Organic laser dyes represent attractive optical materials because they are tunable across the ultraviolet and to the near-infrared. Currently, liquid dye lasers are used which have inherent problems associated with the required solvents and physical pumps to pump dye solutions through resonators to maintain photostability. To overcome problems associated with solutions, laser dyes have been doped into a wide range of matrixes from purely organic polymers[49] to purely inorganic hosts.[50−52] Organic matrixes offer high dye solubility and ease of processing but suffer from poor mechanical and thermal properties whereas inorganic matrixes are generally the opposite. To combine the best properties of both systems, research groups began working with composite materials such as organically modified silicates (ORMOSIL)[77,78] and recently hybrid mesostructured composites.

In 1999, Marlow et al. grew mesostructured fibers doped with a well-investigated laser dye of the xanthene family, rhodamine 6G.[79] Unlike previous studies where simple absorption and fluorescence measurements were performed, they investigated the emission properties as a function of pump intensity. When a single fiber was excited by the second harmonic of a Nd:YAG laser, 532 nm, above excitation intensities of $\sim$15 kW/cm² the emission intensity dramatically increased accompanied by narrowing of the spectrum. These observations are consistent with a form of mirrorless lasing called amplified spontaneous emission (ASE). In ASE, spontaneously emitted photons undergo stimulated emission as they travel down a high gain material, in this case the doped fiber. Above a critical pumping energy, the emission spectrum undergoes gain-narrowing and superlinear output behavior until gain saturation limits the amount of amplification that can be achieved. The final full width at half-maximum (fwhm) is 7−10 nm, as compared to $\sim$60 nm for the photoluminescence spectra well below threshold (Figure 3). Since this process does not provide any feedback, the light emitted at the end of the fiber is usually not spatially and temporally coherent.

The following year, the same research group extended the processing of doped mesostructured materials to more easily processed block copolymer templated film solutions. The film solutions were then patterned into waveguiding structures by soft lithography.[80,81] This
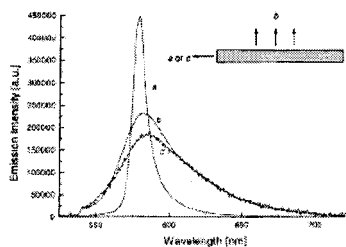
Reviews

Chem. Mater., Vol. 13, No. 10, 2001   3145

Figure 3. Fluorescence spectra of a single fiber (diameter 10 μm by 300 mm long) measured parallel to the fiber axis: (a) gain narrowed spectrum at 150 kW/cm^2; (b) radial emission at 150 kW/cm^2; (c) axial emission at 15 kW/cm^2.

resulted in high-quality mesostructured line patterns, which can be produced within hours (3–12 h) (Figure 4a,b). When the block copolymer P123 [EO$_{20}$–PO$_{70}$–EO$_{20}$] is used as a structure directing agent, the channels of the $p6mm$ mesostructure are preferentially aligned parallel to the substrate and also along the direction of the waveguides. For best results, good waveguiding and flat edges for the emission are required. Flat edges were obtained by aligning the waveguide structures in reference to a cleavage plane on a silicon wafer. However, for good waveguiding, the refractive index of the material must be higher than the support, and for the dye-doped mesostructured material ($n \sim 1.43$) on silicon ($n \sim 3.5$) this is not the case. To solve this problem, a thin mesoporous film ($n \sim 1.15$–1.35) was spun-coated onto the wafer before the dye-doped mesostructured waveguide was produced (Figure 4c,d). When these waveguides are optically pumped with the second harmonic from a Nd:YAG laser (532 nm, 10 Hz), they exhibit ASE. The gain narrowing reduces the final fwhm to 7–8 nm, from $\sim$60 nm of the photoluminescence spectra well below the threshold, similar to the fibers. The ASE threshold depends on the dye concentration and can be as low as $\sim$6–8 kW cm^{-2} at a dye concentration of 1.5 wt %. In contrast, the threshold for sol–gel glasses having the same dye content, but prepared without block copolymer, is more than an order of magnitude higher ($>$200 kW cm^{-2}). These significant differences are attributed to the uniform, high-surface-area mesostructures, which makes it possible to highly disperse and isolate individual R6G molecules. This lowers the number of dimers in the final solid, which is favorable for obtaining a lower threshold laser material, since R6G dimers have low quantum yields.

Feedback for narrow wavelength lasing can be introduced by fabricating one of the many resonator structures. For example, an in-plane Fabry–Perot laser can be made by coating the ends of waveguides with metal or having a significant enough difference in refractive index to cause reflection at the gain material air interface. Another type of resonator that can be made simply by coating a circular dielectric object with a gain material is a micocavity ring laser.[82] This type of resonator has the advantage of having a high Q and low thresholds because a large percentage of spontaneously emitted photons undergo stimulated emission.[83] Using the microcavity ring laser design, optical fibers (40–125 μm diameter) were first coated with a mesoporous thin film by dip-coating followed by calcination. Similarly to the multilayer waveguiding structure described
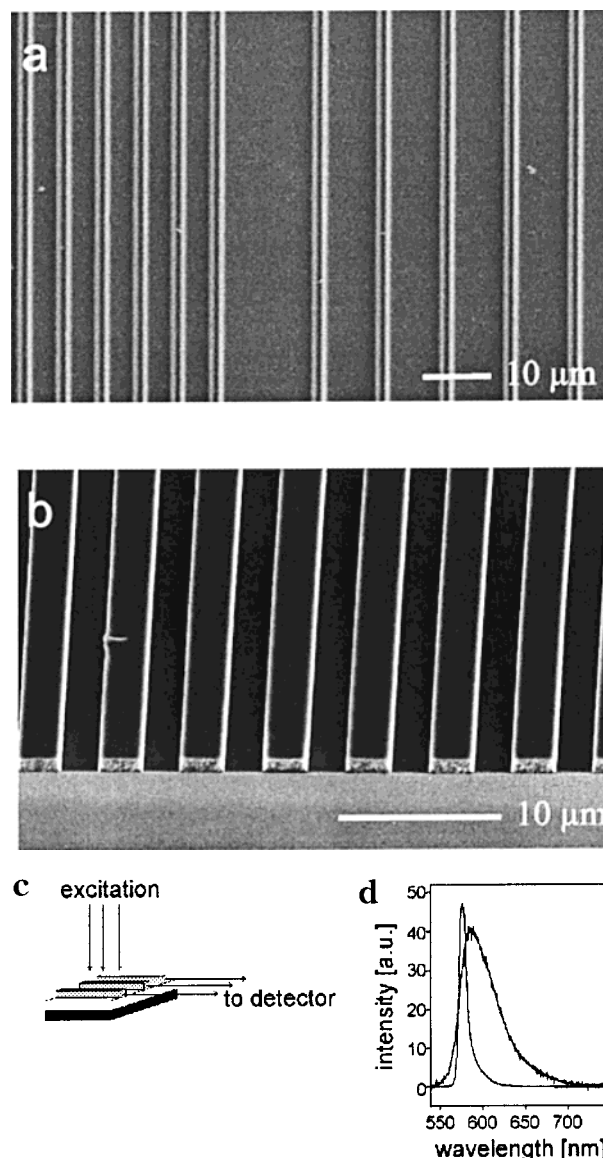

Figure 4. (a, b) SEM image of mesostructured waveguides. (c) Schematic of waveguide geometry with pumping and emission collection. (d) Typical luminescence spectrum below and above threshold.

previously, the thin mesoporous film acts as a low refractive index support. The lasing layer is then dip-coated onto this support. When optically pumped, a fraction of the emitted light is confined to the outer layer and travels around the microring. When the pumping energy reaches a certain threshold, the gain becomes greater than the loss and lasing is observed at the frequencies given by the condition $\Delta\nu = c/d\pi n_{\text{eff}}$ ($n_{\text{eff}} \sim n \sim 1.43$) (Figure 5).[84] A detailed analysis of the lasing spectrum reveals that the waveguided modes are further modulated by whispering galley modes, which are modes travelling near the outer surface of the dye-doped layer and do not reach the mesoporous film/mesostructured film interface. The lasing threshold for these microring configuration ranges from $\sim$1.5 kW cm^{-2} for 125 μm fibers to as low as $\sim$0.4 kW cm^{-2} on a 40 μm fiber. Also, as the threshold is reduced, the number of lasing modes is reduced from $>$50 to $<$10. We note that $\sim$0.4 kW cm^{-2} compares well with semiconducting polymers ($\sim$0.5–0.01 kW cm^{-2} for the best compounds).
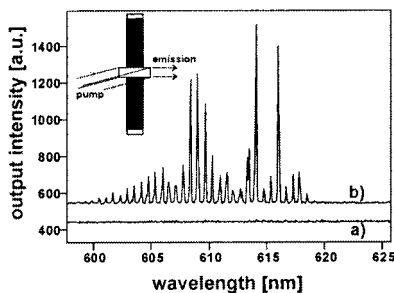
Figure 5. (a) Luminescence spectrum at low pump intensities (<1 kW/cm^2). (b) Luminescence spectrum above threshold (6 kW/cm^2). Inset depicts measurement geometry.

Furthermore, using smaller fibers and achieving single mode operation can be expected to further reduce the threshold. Although these structures are easy to fabricate, they are less convenient to integrate into devices because they emit light in a ring normal to the fiber axis instead of a well-defined beam.

One way to make an in-plane laser with a well-defined output beam is to reflect light into a waveguide through the incorporation of a periodic modulation of refractive index or gain so that light is Bragg reflected. Lasers that operate by this type of grating induced coupling are known as distributed feedback (DFB) lasers.[82] The lasing wavelength of a DFB laser is close to the Bragg wavelength, $\lambda_{Bragg} = 2 n_{eff} \Lambda$ (n_{eff} is the effective refractive index of the waveguide and Λ is the period of the grating), and can be tuned by changing either n_{eff} or Λ. Single mode DFB lasers are made when light is reflected through modulation of gain or by incorporating a phase shift, whereas dual mode DFB lasers are obtained when Bragg reflection occurs through modulating the refractive index with one mode just below and the other just above λ_{Bragg}.[85]

Once again, soft lithography is used to pattern mesostructured materials.[86] However, instead of a smooth waveguide, a periodic grating is created on the top structure. Samples are optically pumped with a small stripe perpendicular to the grooves in the ridge waveguides by a frequency-doubled Nd:YAG laser at 532 nm and 10 Hz. Below threshold, the emission is characteristic of spontaneous emission and broad, ~60 nm. Once threshold is reached, ~55 kW/cm^2, the emission is dominated by a few narrow lines from DFB lasing. Unfortunately, the threshold is higher than ASE in patterned waveguide structures of similar composition, ~10 kW/cm^2.[81] Differences are assigned to the quality of the grating. This assessment is reinforced by analysis of the emission spectra. Unlike the one or two lasing modes predicted by theory, most samples have 4–5 modes (Figure 6). Multimode behavior most likely results from slight distortions in the grating period over the pumped region. These distortions are assigned either to the master/stamp production or from the transfer of the pattern by the stamps to the mesostructure. To produce the first-order Bragg grating used to provide feedback in these samples, a small period is required, ~200 nm. While soft lithography has successfully fabricated structures smaller than 200 nm, single mode lasing places stringent requirements on exact periodicity, and small deformations associated with soft
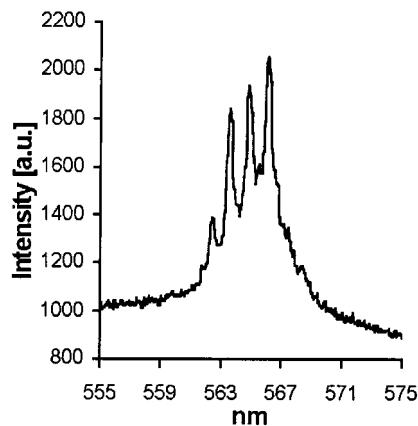

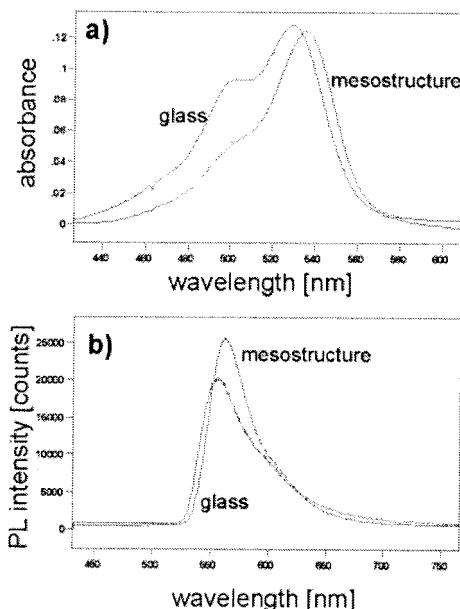**Figure 6.** Typical lasing spectrum for DFB laser.

Figure 7. (a) Absorption spectra of rhodamine 6G occluded in a mesostructured block copolymer/silica composites and in a sol–gel glass (0.5 wt %) and (b) corresponding emission spectra. Note that due to the lower quantum efficiency, the emission spectrum of the dye-doped sol–gel glass was multiplied for easier comparison.

lithography itself could change the grating period enough to observe this behavior.[87] Previous studies on stamped organic DFBs used higher order gratings therefore having longer periods and still observed multimode mode behavior in many samples.[88,89] Another possible explanation is that the large size of the excitation beam simultaneously excites multiple waveguides. For example, in Figure 6 each waveguide is 3 μm wide and separated by 4 μm so a 0.5 mm wide excitation strip would excite ~72 DFBs. Therefore, if there were a small difference between each waveguide DFB, then multiple emission peaks would be observed.

We now turn to the question of why mesostructured silica/block copolymer composites are well suited for lasing applications. To gain insight, analyses were performed on both the UV/vis absorption and emission spectra as well as the quantum yields of R6G-doped thin films in direct comparison to R6G-doped sol–gel glasses.[90] Figure 7 depicts typical absorption and emission spectra for R6G occluded in a *p6mm* mesostructured and pure SiO$_2$ thin films. The dye concentration in the solids is

the same for both samples (0.5 wt %). Several features are evident from the spectra: In the absorption spectra, two absorption bands are evident. The first peak at 530 nm for R6G occluded in sol−gel silica, whereas this peak is shifted to about 536 nm in the mesostructured host (Figure 7). This red shift is also observed in the corresponding emission spectra. The wavelength shift was attributed to a change in the environment due to the additional presence of the block copolymer, which interacts with the dye molecules. Moreover, absorption spectra reveal that the dimer band at about 502 nm in the case of the sol−gel glass (507 nm for the mesostructured host) is much more pronounced in the former case. Hence, dimerization of the dye molecules is considerably reduced in mesostructured materials. An explanation for this finding is that the dye molecules coassemble within the hydrophobic domain of the block copolymers or are occluded in the PEO domain. The block copolymer−dye interaction leads to a high dispersion of the occluded dyes since the probability for dye−dye interaction is reduced. Since it is known that R6G dimers have much lower quantum efficiencies than monomers, this also explains and underlines the superior lasing properties for R6G-doped mesostructured materials. This is further supported by quantum efficiency measurements which quantitatively demonstrate that dimerization for R6G is largely reduced in block copolymer/silica nanocomposites in comparison to pure sol−gel SiO$_2$ glasses. A systematic investigation for R6G concentrations from 0.1 to 2.5 wt % clearly demonstrates that, with increasing dye concentration, the quantum efficiencies decrease. However, for all concentrations investigated, the quantum efficiencies of the mesostructured materials are significantly higher (by at least an order of magnitude) than those of the dye-doped sol−gel glasses. This finding clearly underlines the conclusion from the UV/vis absorption spectra that the R6G dye molecules are much better isolated within these mesostructured organic/inorganic nanocomposites. The higher quantum efficiencies also explain the significantly lower thresholds for lasing in these novel systems.

Photochromic Materials

Mesostructured materials can also host photochromic dyes, i.e., dyes that change their color upon light illumination.[91] For spiropyrane and spirooxazine derivatives, this is due to ring opening of the molecules upon light irradiation, producing a color change. For applications, it is desirable that the reverse reaction (thermal bleaching) is fast, which allows rapid switching between two states (high/low transmission in a certain wavelength range). Inorganic, organic, and mixed inorganic/organic materials have been investigated as matrices. For purely inorganic host materials, the response times are slow in comparison to solution (minutes vs seconds), and undesired reverse photochromism is often observed in these matrices. In organic matrices, on the other hand, the response can be much faster (on the order of seconds).[92] However, pure organic materials like PMMA possess lower thermal stability and mechanical robustness than glasses. In these matrices more than one site is available for the dye, which then results in a multiple distribution of response times. The properties can be improved, however, by
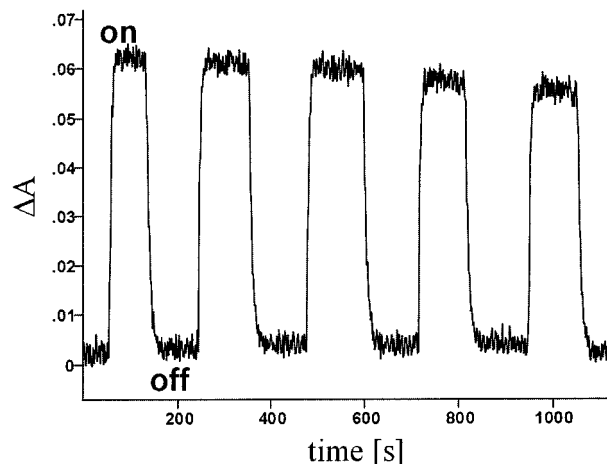

Figure 8. Photochromic mesostructured thin films doped with a spirooxazine. Transmission of the thin films during several on/off cycles.

blending inorganic and organic components on a molecular level. A bleaching constant of 0.2 s^{-1} was reported for a spirooxazine molecule embedded in a organically modified silicate, which is as fast as the response time of the same dye in ethanol solution.[93]

In this context, mesostructured block copolymer/silica composites were explored, since a priori they were expected to be excellent hosts to provide the materials base for the requirements discussed above.[94] Thin films were prepared by dip-coating dye-doped precursor solutions. When doped with 1,3-dihydro-1,3,3-trimethylspiro-[2H-indole-2,3′-[3H]naphth[2,1-b][1,4]oxazine], a spirooxazine derivative, the thin films are colorless and exhibit a transmission of ∼100% throughout the visible spectrum. However, when the thin films are illuminated with 355 nm light from an UV lamp, they become immediately blue. Upon removal of the light source, they become completely colorless again, the entire thermal back-fading process taking only a few seconds (Figure 8).

A detailed analysis of the bleaching kinetics revealed a rate constant for back-fading $k = 0.15$ s^{-1}, which compares well to the best value reported for this molecule in a solid matrix.[93] The bleaching curves can be fit by monoexponential functions, indicating a homogeneous dye environment. On the basis of the fact that the dye exhibits only normal photochromism, it was concluded that the dye was located within the organic part of the composite, most probably within the PEO subdomain. This is supported by the fact that, in sol−gel glasses prepared without block copolymers, the same dye (i) shows a much slower response and (ii) begins to exhibit reverse photochromism (compounds are colored in the dark and become colorless upon light illumination) after prolonged aging. This is attributed to a stabilization of the open form by the silica host through hydrogen bonding. Here, it is interesting to note that the rate constant for back-fading of the spirooxazine increases with prolonged aging time of the thin films. Whereas $k = 0.09$ s^{-1} for fresh films (2 days old), k increases to 0.15 s^{-1} for 3 week old films. This demonstrates that hydrolysis and condensation of the SiO$_2$ network is ongoing during this aging process. As a consequence, the number of hydroxyl groups on the silica surface is reduced, providing fewer

hydrogen binding sites for the open form of the dye.

These data strongly suggest that upon direct doping of mesostructured silica/block copolymer composites with spriooxazine and spiropyrane molecules, the latter predominantly coassemble with the block copolymer and are finally located within the organic part of the composite. This makes these materials different from purely inorganic SiO_2 sol−gel glasses as evidenced by the different spectral properties of the occluded dyes and demonstrates that a more sophisticated local-environment tuning is offered by mesostructured materials.

Chemical Sensors

Their highly porous nature combined with low absorption and emission in the visible spectrum makes mesoporous materials excellent candidates for optical sensors. Formerly, sensing based on optical detection has been implemented in sol−gel glasses. Typically, these sensors are operated by measuring the transmission, emission, or lifetime of a complex or an organic dye embedded in a SiO_2 matrix. Two important considerations in developing an optical sensor are the occlusion of the sensing dye/complex (physical occlusion vs covalent anchoring) and the diffusion times of the target analyte, which are determined by the glass microstructure. Whereas the first point is important to leaching and hence to long-term operation, the second point determines the response times. Principally, the requirements of fast response and negligible leaching can be fulfilled advantageously in large-pore mesoporous materials by covalently anchoring the active sensor dye during synthesis and low-temperature removal of the structure directing agent afterward.

On the basis of this consideration, simultaneously, two research groups developed pH sensors based on covalently linked fluorescein derivatives, a pH-sensitive dye. Wirnsberger et al. synthesized a sensor by reacting fluorescein isothiocyanate with 3-aminopropyltriethoxysilane and adding to a F127 block copolymer film preparation.[95] This functionalization ensures that the dye is covalently anchored onto (or within) the SiO_2 wall during mesostructure synthesis. After dip-coating, the ~900 nm thick films were dried for about 10 days at room temperature and finally at 70 °C for 3−5 days. This prolonged drying treatment is necessary in order to achieve a sufficiently high robustness of the thin films before block copolymer extraction by ethanol at 80 °C. Otherwise, the films exhibit severe cracking after extraction, which limits their use in optical sensing devices.

The sensor operates by recording the emission of the anchored dye. In Figure 9a, a typical plot of the emission spectra upon bringing the thin film into contact with solutions of different pH values is given. Similarly to what is observed for fluorescein in solution, the integrated emission increases with increasing pH. A typical plot of the emission vs the pH (Figure 9b) clearly demonstrates that the thin film sensors act analogously to the dye in solution, except that the pK_a value is shifted from 6.4 in solution to ~7.3 in the thin films. In comparison to solution, a broadening of the titration curve is evident. This is attributed to two factors: First, an inhomogeneous dye environment may contribute to this broadening. Second, fluorescein possesses three pK_a
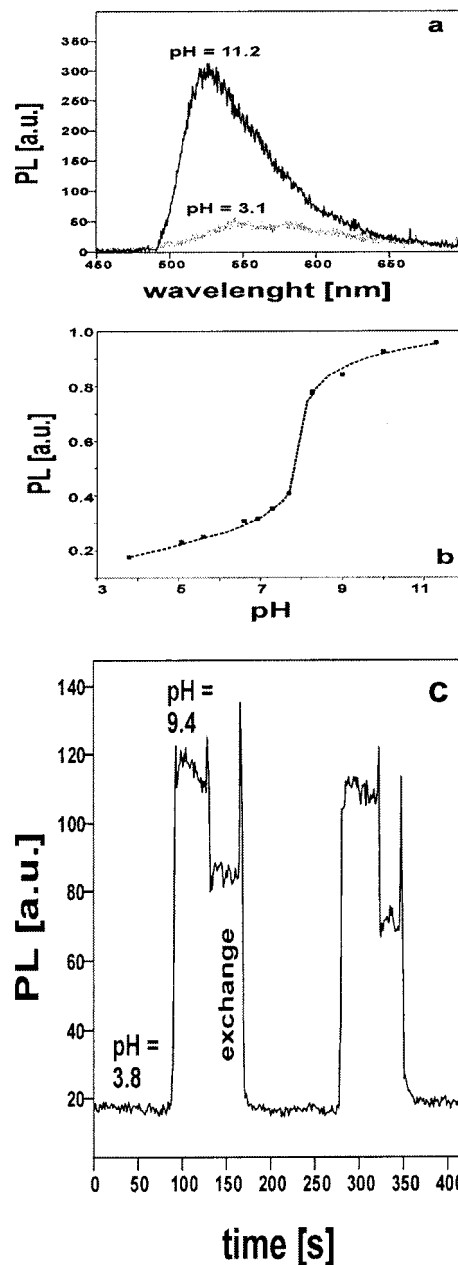

Figure 9. pH sensing with a fluorescein-doped, mesoporous thin film: (a) photoluminescence spectra at pH = 3.1 and pH = 11.2; (b) titration curve; (c) change of photoluminescence upon exchange of pH buffer solutions, demonstrating immediate response of the thin films.

values ($pK_{a,1}$ = 2.08, $pK_{a,2}$ = 4.31, $pK_{a,3}$ = 6.43) which are often difficult to distinguish even in solution.

The response time of the thin films is on the order of ~7 s for a 95% change in the emission intensity (see Figure 9c for a typical example). In sol−gel glasses, the response times are much longer than this value, the only exception being small capillaries coated with sol−gel glasses. The fast response time was attributed to the high porosity of the dye carrying mesoporous thin film, since the open pores enable a fast diffusion of the solution toward the dye molecules.

Another research group led by Brinker and co-workers used a more elaborate approach involving microfluidics to produce a similar pH sensor.[96] They first patterned amine modified cubic mesoporous silica using selective dewetting of patterned surfaces made by surface as-
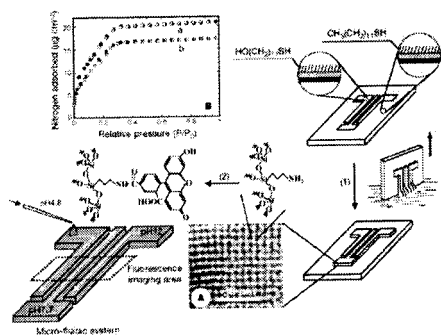
Figure 10. Scheme for patterned functionalize mesoporous materials formed by selective dewetting using SAMs. Gas adsorption−desorption isotherms and TEM confirm cubic structure in film and reduction in surface area with dye attachment (curve b).

sembled monolayers (SAMs). The patterned consisted of three L-shaped patterns with a viewing cell created by interdigitating long narrow lines with large pads on the ends used to load solutions (Figure 10). The surfactant was removed by calcination while maintaining both the amine functionality, as confirmed by NMR, and high surface area measured by gas adsorption. Fluorescein succinamide was covalently attached and the patterned mesoporous surface extensively washed to remove unreacted dye. Finally, solutions of different pH were placed on the pads and transported to the imagining cell by capillary flow. Fluorescence studies showed that the dye-modified materials were active as pH sensors and gave relative intensities similar to the dye in solutions. This application clearly demonstrates that these mesoporous, highly ordered, and transparent thin films of high mechanical robustness are well-suited materials for fast response optical sensors.

Conclusions and Outlook

Mesoporous and mesostructured materials derived by a combination of surfactant/block copolymer templating sol−gel chemistry are attractive candidates for optical applications such as lasers, optical sensors, photochromic materials, and host for quantum confined structures. Under weakly acidic conditions, they can be processed similarly to sol−gel glasses, allowing for a wide variety of macroscopic shapes. The main differences compared to sol−gel glasses are the ordered sequence of either surfactant or block copolymer/silica or holes (pores)/silica on the nanometer scale. The high porosity of calcined mesoporous materials offers new possibilities for new optical sensor components because of the high surface accessible by vapors and liquids. pH sensing is a first example; however, other sensing applications in the fields of vapor composition, O_2 content in water, or biosensors, etc., can be envisioned. We expect that the combination of the sensing capabilities together with fast processing techniques and pattern recognition will lead to optical-based multiple-sensor arrays, which can evaluate the composition of vapors and liquids in the microsecond domain.

Mesoporous and mesostructured materials are very efficient for dye doping. Dyes can be incorporated at high concentrations while still having isolated dye molecules in the final solids, a property that is useful in creating low-threshold laser materials and fast-response photochromic composites with a large change

in absorption. Moreover, in the mesostructured block copolymer/silica composites, the block copolymers determine the local molecular environment of the occluded dyes. The latter property will be useful for constructing more complex composite materials. For example, one could envision an energy-transfer system, in which the block copolymer (or surfactant) carries an optically active unit, which transfers energy to a nearby located dye after excitation.

Mesoporous materials have been shown to be excellent host for synthesizing quantum confined structures. The ability to tailor the pore size and loading conditions offer the ability to produce nanocrystals of both direct and indirect semiconductors. When the loading techniques are perfected, mesoporous materials will make it possible to produce highly ordered arrays of quantum dots, which could be useful for applications such as quantum dot lasers. Ordered arrays of isolated MEH-PPV chains have already shown to be successful at controlling the flow of energy from outside the mesoporous silica to the channels. Finally, by investigating the optical and or electrical properties of the transition metal oxides or metal sulfides, new optoelectronic devices are certainly possible. As one example currently being pursued in a number of laboratories, using ordered mesoporous titania in place of sintered titania should allow for higher dye loading and higher efficiency for solar cells.[97]

References

(1) Yanagisawa, T.; Shimizu, T.; Kuroda, K.; Kato, C. *Bull. Chem. Soc. Jpn.* **1990**, *63*, 988−992.
(2) Kresge, C. T.; Leonowicz, M. E.; Roth, W. J.; Vartuli, J. C.; Beck, J. S. *Nature* **1992**, *359*, 710−712.
(3) Zhao, D. Y.; Feng, J. L.; Huo, Q. S.; Melosh, N.; Fredrickson, G. H.; Chmelka, B. F.; Stucky, G. D. *Science* **1998**, *279*, 548−552.
(4) Schmidt-Winkel, P.; Lukens, W. W.; Zhao, D. Y.; Yang, P. D.; Chmelka, B. F.; Stucky, G. D. *J. Am. Chem. Soc.* **1999**, *121*, 254−255.
(5) Yang, P. D.; Zhao, D. Y.; Margolese, D. I.; Chmelka, B. F.; Stucky, G. D. *Nature* **1998**, *396*, 152−155.
(6) Ciesla, U.; Demuth, D.; Leon, R.; Petroff, P.; Stucky, G.; Unger, K.; Schuth, F. *J. Chem. Soc., Chem. Commun.* **1994**, 1387−1388.
(7) Ciesla, U.; Schacht, S.; Stucky, G. D.; Unger, K. K.; Schuth, F. *Angew. Chem., Int. Ed. Engl.* **1996**, *35*, 541−543.
(8) Antonelli, D. M.; Nakahira, A.; Ying, J. Y. *Inorg. Chem.* **1996**, *35*, 3126−3136.
(9) Antonelli, D. M.; Ying, J. Y. *Angew. Chem., Int. Ed. Engl.* **1996**, *35*, 426−430.
(10) MacLachlan, M. J.; Coombs, N.; Ozin, G. A. *Nature* **1999**, *397*, 681−684.
(11) MacLachlan, M. J.; Coombs, N.; Bedard, R. L.; White, S.; Thompson, L. K.; Ozin, G. A. *J. Am. Chem. Soc.* **1999**, *121*, 12005−12017.
(12) Braun, P. V.; Osenar, P.; Stupp, S. I. *Nature* **1996**, *380*, 325−328.
(13) Braun, P. V.; Osenar, P.; Tohver, V.; Kennedy, S. B.; Stupp, S. I. *J. Am. Chem. Soc.* **1999**, *121*, 7302−7309.
(14) Rangan, K. K.; Billinge, S. J. L.; Petkov, V.; Heising, J.; Kanatzidis, M. G. *Chem. Mater.* **1999**, *11*, 2629−2632.
(15) Li, J. Q.; Nazar, L. F. *Chem. Commun.* **2000**, 1749−1750.

(16) Melde, B. J.; Holland, B. T.; Blanford, C. F.; Stein, A. *Chem. Mater.* **1999**, *11*, 3302–3308.
(17) Yoshina-Ishii, C.; Asefa, T.; Coombs, N.; MacLachlan, M. J.; Ozin, G. A. *Chem. Commun.* **1999**, 2539–2540.
(18) Inagaki, S.; Guan, S.; Fukushima, Y.; Ohsuna, T.; Terasaki, O. *J. Am. Chem. Soc.* **1999**, *121*, 9611–9614.
(19) Lu, Y. F.; Fan, H. Y.; Doke, N.; Loy, D. A.; Assink, R. A.; LaVan, D. A.; Brinker, C. J. *J. Am. Chem. Soc.* **2000**, *122*, 5258–5261.
(20) Zhao, D. Y.; Yang, P. D.; Margolese, D. I.; Chmelka, B. F.; Stucky, G. D. *Chem. Commun.* **1998**, 2499–2500.
(21) Brinker, C. J.; Lu, Y. F.; Sellinger, A.; Fan, H. Y. *Adv. Mater.* **1999**, *11*, 579–585, 514.
(22) Ogawa, M. *Chem. Commun.* **1996**, 1149–1150.
(23) Ryoo, R.; Ko, C. H.; Cho, S. J.; Kim, J. M. *J. Phys. Chem. B* **1997**, *101*, 10610–10613.
(24) Yang, H.; Coombs, N.; Sokolov, I.; Ozin, G. A. *Nature* **1996**, *381*, 589–592.
(25) Yang, H.; Kuperman, A.; Coombs, N.; Mamicheafara, S.; Ozin, G. A. *Nature* **1996**, *379*, 703–705.
(26) Huo, Q. S.; Zhao, D. Y.; Feng, J. L.; Weston, K.; Buratto, S. K.; Stucky, G. D.; Schacht, S.; Schuth, F. *Adv. Mater.* **1997**, *9*, 974+.
(27) Melosh, N. A.; Lipic, P.; Bates, F. S.; Wudl, F.; Stucky, G. D.; Fredrickson, G. H.; Chmelka, B. F. *Macromolecules* **1999**, *32*, 4332–4342.
(28) Attard, G. S.; Glyde, J. C.; Goltner, C. G. *Nature* **1995**, *378*, 366–368.
(29) Feng, P. Y.; Bu, X. H.; Stucky, G. D.; Pine, D. J. *J. Am. Chem. Soc.* **2000**, *122*, 994–995.
(30) Sokolov, I.; Yang, H.; Ozin, G. A.; Kresge, C. T. *Adv. Mater.* **1999**, *11*, 636–642, 596.
(31) Yang, S. M.; Sokolov, I.; Coombs, N.; Kresge, C. T.; Ozin, G. A. *Adv. Mater.* **1999**, *11*, 1427–1431.
(32) Doshi, D. A.; Huesing, N. K.; Lu, M. C.; Fan, H. Y.; Lu, Y. F.; Simmons-Potter, K.; Potter, B. G.; Hurd, A. J.; Brinker, C. J. *Science* **2000**, *290*, 107–111.
(33) Yang, P. D.; Deng, T.; Zhao, D. Y.; Feng, P. Y.; Pine, D.; Chmelka, B. F.; Whitesides, G. M.; Stucky, G. D. *Science* **1998**, *282*, 2244–2246.
(34) Trau, M.; Yao, N.; Kim, E.; Xia, Y.; Whitesides, G. M.; Aksay, I. A. *Nature* **1997**, *390*, 674–676.
(35) Zhao, D.; Yang, P.; Melosh, N.; Feng, J.; Chmelka, B. F.; Stucky, G. D. *Adv. Mater.* **1998**, *10*, 1380–1385.
(36) Parala, H.; Winkler, H.; Kolbe, M.; Wohlfart, A.; Fischer, R. A.; Schmechel, R.; von Seggern, H. *Adv. Mater.* **2000**, *12*, 1050–1055.
(37) Srdanov, V. I.; Alxneit, I.; Stucky, G. D.; Reaves, C. M.; DenBaars, S. P. *J. Phys. Chem. B* **1998**, *102*, 3341–3344.
(38) Winkler, H.; Birkner, A.; Hagen, V.; Wolf, I.; Schmechel, R.; von Seggern, H.; Fischer, R. A. *Adv. Mater.* **1999**, *11*, 1444–1448.
(39) Hirai, T.; Okubo, H.; Komasawa, I. *J. Phys. Chem. B* **1999**, *103*, 4228–4230.
(40) Zhang, W. H.; Shi, J. L.; Wang, L. Z.; Yan, D. S. *Chem. Mater.* **2000**, *12*, 1408–1413.
(41) Agger, J. R.; Anderson, M. W.; Pemble, M. E.; Terasaki, O.; Nozue, Y. *J. Phys. Chem. B* **1998**, *102*, 3345–3353.
(42) Han, Y. J.; Kim, J. M.; Stucky, G. D. *Chem. Mater.* **2000**, *12*, 2068–2069.
(43) Ko, C. H.; Ryoo, R. *Chem. Commun.* **1996**, 2467–2468.
(44) Huang, M. H.; Choudrey, A.; Yang, P. D. *Chem. Commun.* **2000**, 1063–1064.
(45) For reviews see: (a) Reisfeld, R. *Struct. Bonding* **1996**, *85*, 215–234. (b) Lebeau, B. Sanchez, C. *Curr. Opin. Solid State Mater. Sci.* **1999**, *4*, 11–23. (c) Avnir, D. *Acc. Chem. Res.* **1995**, *39*, 328–334.
(46) Ying, J. Y.; Mehnert, C. P.; Wong, M. S. *Angew. Chem., Int. Ed. Engl.* **1999**, *38*, 56–77.
(47) Corma, A. *Chem. Rev.* **1997**, *97*, 2373–2419.
(48) For general reviews: (a) Ihlein, G.; Junges, B.; Junges, U.; Laeri, F.; Schuth, F.; Vietze, U. *Appl. Organomet. Chem.* **1998**, *12*, 305–314. (b) Ramamurthy, V.; Eaton, D. F. *Chem. Mater.* **1994**, *6*, 1128–1136. For second harmonic generation papers see: (c) Cox, S. D.; Gier, T. E.; Stucky, G. D. *Chem. Mater.* **1990**, *2*, 609–619. (d) Marlow, F.; Caro, J.; Werner, L.; Kornatowski, J.; Dahne, S. *J. Phys. Chem.* **1993**, *97*, 11286–11290. (e) Marlow, F.; Caro, J. *Mol. Cryst. Liq. Cryst. Sci. Technol., Sect. A: Mol. Cryst. Liq. Cryst.* **1994**, *240*, 175–181. (f) Werner, L.; Caro, J.; Finger, G.; Kornatowski, J. *Zeolites* **1992**, *12*, 658–663. (g) Marlow, F.; Caro, J. *Zeolites* **1992**, *12*, 433–434. For lasers and luminescence see: (h) Vietze, U.; Krauss, O.; Laeri, F.; Ihlein, G.; Schuth, F.; Limburg, B.; Abraham, M. *Phys. Rev. Lett.* **1998**, *81*, 4628–4631. (i) Ihlein, G.; Schuth, F.; Krauss, O.; Vietze, U.; Laeri, F. *Adv. Mater.* **1998**, *10*, 1117+. (j) Braun, I.; Ihlein, G.; Laeri, F.; Nockel, J. U.; Schulz-Ekloff, G.; Schuth, F.; Vietze, U.; Weiss, O.; Wohrle, D. *Appl. Phys. B: Lasers Opt.* **2000**, *70*, 335–343. (k) Caro, J.; Marlow, F.; Wubbenhorst, M. *Adv. Mater.* **1994**, *6*, 413–416.
(49) Hermes, R.; Allik, T. H.; Chandra, S.; Hutchinson, J. A. *Appl. Phys. Lett.* **1993**, *63*, 877–879.
(50) Avnir, D.; Levy, D.; Reisfeld, R. *J. Phys. Chem.* **1984**, *88*, 5956–5959.
(51) Reisfeld, R.; Brusilovsky, D.; Eyal, M.; Miron, E.; Burstein, Z.; Ivri, J. *Chem. Phys. Lett.* **1989**, *160*, 43–44.
(52) Dunn, B.; Zink, J. I. *J. Mater. Chem.* **1991**, *1*, 903–913.
(53) Zhou, H. S.; Honma, I. *Chem. Lett.* **1998**, 973–974.
(54) Zhou, H. S.; Sasabe, H.; Honma, I. *J. Mater. Chem.* **1998**, *8*, 515–516.
(55) Zhou, H. S.; Honma, I. *Adv. Mater.* **1999**, *11*, 683–685, 598.
(56) Hoppe, R.; Ortlam, A.; Rathousky, J.; Schulz-Ekloff, G.; Zukal, A. *Microporous Mater.* **1997**, *8*, 267–273.
(57) Yamashita, H.; A, T.; Nishimura, M.; Koyano, K.; Tatsumi, T.; Anpo, M. *Stud. Surf. Sci. Catal.* **1998**, *117*, 551–558.
(58) Gu, G.; Ong, P. P.; Li, Q. T. *J. Phys. D: Appl. Phys.* **1999**, *32*, 2287–2289.
(59) Fowler, C. E.; Lebeau, B.; Mann, S. *Chem. Commun.* **1998**, 1825–1826.
(60) Lebeau, B.; Fowler, C. E.; Hall, S. R.; Mann, S. *J. Mater. Chem.* **1999**, *9*, 2279–2281.
(61) Ganschow, M.; Wark, M.; Wohrle, D.; Schulz-Ekloff, G. *Angew. Chem., Int. Ed. Engl.* **2000**, *39*, 161–163.
(62) Shibata, M.; Hotta, H.; Suzuki, T.; Valange, S.; Gabelica, Z. *Chem. Lett.* **1999**, 1291–1292.
(63) Horino, M. Japanese Patent 53-113036, 1978.
(64) Alivisatos, A. P. *J. Phys. Chem.* **1996**, *100*, 13226–13239.
(65) Leon, R.; Margolese, D.; Stucky, G.; Petroff, P. M. *Phys. Rev. B: Condens. Matter Mater. Phys.* **1995**, *52*, R2285–R2288.
(66) Dag, O.; Ozin, G. A.; Yang, H.; Reber, C.; Bussiere, G. *Adv. Mater.* **1999**, *11*, 474–480.
(67) Murray, C. B.; Norris, D. J.; Bawendi, M. G. *J. Am. Chem. Soc.* **1993**, *115*, 8706–8715.
(68) Ogawa, M.; Nakamura, T.; Mori, J.; Kuroda, K. *J. Phys. Chem. B* **2000**, *104*, 8554–8556.
(69) Xu, Q. H.; Li, L. S.; Li, B.; Yu, J. H.; Xu, R. R. *Microporous Mesoporous Mater.* **2000**, *38*, 351–358.
(70) Blasse, G.; Briel, A.; Niewport, W. C. *J. Phys. Chem. Solids* **1966**, *27*, 1587.
(71) Jorgenson, C. K.; Judd, B. R. *Mol. Phys.* **1964**, *8*, 281.
(72) Tolbert, S. H.; Firouzi, A.; Stucky, G. D.; Chmelka, B. F. *Science* **1997**, *278*, 264–268.
(73) Wu, J. J.; Gross, A. F.; Tolbert, S. H. *J. Phys. Chem. B* **1999**, *103*, 2374–2384.
(74) Nguyen, T. Q.; Wu, J. J.; Doan, V.; Schwartz, B. J.; Tolbert, S. H. *Science* **2000**, *288*, 652–656.
(75) Marlow, F. *Mol. Cryst. Liq. Cryst.* **2000**, *341*, 1093–1098.
(76) Kinski, I.; Gies, H.; Marlow, F. *Zeolites* **1997**, *19*, 375–381.
(77) Viana, B.; Koslova, N.; Aschehoug, P.; Sanchez, C. *J. Mater. Chem.* **1995**, *5*, 719–724.
(78) Canva, M.; Georges, P.; Perelgritz, J. F.; Brum, A.; Chaput, F.; Boilot, J. P. *Appl. Opt.* **1995**, *34*, 428–431.
(79) Marlow, F.; McGehee, M. D.; Zhao, D. Y.; Chmelka, B. F.; Stucky, G. D. *Adv. Mater.* **1999**, *11*, 632–636.
(80) Xia, Y. N.; Whitesides, G. M. *Angew. Chem., Int. Ed. Engl.* **1998**, *37*, 551–575.
(81) Yang, P. D.; Wirnsberger, G.; Huang, H. C.; Cordero, S. R.; McGehee, M. D.; Scott, B.; Deng, T.; Whitesides, G. M.; Chmelka, B. F.; Buratto, S. K.; Stucky, G. D. *Science* **2000**, *287*, 465–467.
(82) Dodabalapur, A.; Berggren, M.; Slusher, R. E.; Bao, Z.; Timko, A.; Schiortino, P.; Laskowski, E.; Katz, H. E.; Nalamasu, O. *IEEE J. Select. Top. Quantum Electron.* **1998**, *4*, 67–74.
(83) Yamamoto, Y.; Slusher, R. E. *Phys. Today* **1993**, *46*, 66–73.
(84) Wirnsberger, G.; Stucky, G. D. *Chem. Mater.* **2000**, *12*, 2525–2527.
(85) Coldren, L. A.; Corzine, S. W. *Diode Lasers and Photonic Integrated Circuits*; Wiley: New York, 1995.
(86) Scott, B. J.; Wirnsberger, G.; McGehee, M. D.; Chmelka, B. F.; Stucky, G. D. *Adv. Mater.* **2001**, *13*, 1231–1234.
(87) Rogers, J. A.; Paul, K. E.; Whitesides, G. M. *J. Vac. Sci. Technol. B* **1998**, *16*, 88–97.
(88) Rogers, J. A.; Meier, M.; Dodabalapur, A. *Appl. Phys. Lett.* **1998**, *73*, 1766–1768.
(89) Rogers, J. A.; Meier, M.; Dodabalapur, A.; Laskowski, E. J.; Cappuzzo, M. A. *Appl. Phys. Lett.* **1999**, *74*, 3257–3259.
(90) Wirnsberger, G.; Yang, P. D.; Huang, H. C.; McGehee, M. D.; Scott, B.; Chmelka, B. F.; Stucky, G. D., in press.
(91) Brown, G. H. *Photochromism*; Wiley-Interscience: New York, 1971.
(92) Levitus, M.; Aramendia, P. F. *J. Phys. Chem. B* **1999**, *103*, 1864–1870.
(93) Schaudel, B.; Guermeur, C.; Sanchez, C.; Nakatani, K.; Delaire, J. A. *J. Mater. Chem.* **1997**, *7*, 61–65.
(94) Wirnsberger, G.; Scott, B. J.; Chmelka, B. F.; Stucky, G. D. *Adv. Mater.* **2000**, *12*, 1450–1454.
(95) Wirnsberger, G.; Scott, B. J.; Stucky, G. D. *Chem. Commun.* **2001**, 119–120.
(96) Fan, H. Y.; Lu, Y. F.; Stump, A.; Reed, S. T.; Baer, T.; Schunk, R.; Perez-Luna, V.; Lopez, G. P.; Brinker, C. J. *Nature* **2000**, *405*, 56–60.
(97) Hagfeldt, A.; Gratzel, M. *Acc. Chem. Res.* **2000**, *33*, 269–277.